Efficient Industrial-Current-Density Acetylene to Polymer-Grade Ethylene via Hydrogen-Localization Transfer over Fluorine-Modified Copper

Lei Bai, Yi Wang, Zheng Han, Jinbo Bai, Kunyue Leng, Lirong Zheng, Yunteng Qu, Yuen Wu

Efficient Industrial-Current-Density Acetylene to Polymer-Grade Ethylene via Hydrogen-Localization Transfer over Fluorine-Modified Copper

Lei Bai[1], Yi Wang[1], Zheng Han[1], Jinbo Bai[2], Kunyue Leng[1]*, Lirong Zheng[3*], Yunteng Qu[1]* and Yuen Wu [4]

[1]*International Collaborative Center on Photoelectric Technology and Nano Functional Materials, Institute of Photonics and Photon-Technology, Northwest University, Xi'an, Shaanxi 710069, China*

[2]*Université Paris-Saclay, CentraleSupélec, ENS Paris-Saclay, CNRS, LMPS-Laboratoire de Mécanique Paris-Saclay, 8-10 rue Joliot-Curie, Gif-sur-Yvette 91190, France*

[3]*Institute of High Energy Physics, Beijing 100039, China*

[4]*School of Chemistry and Materials Science, University of science and Technology of China, Hefei 230026, China*

Keywords: Acetylene semihydrogenation, Electrocatalyst, Ethylene production

Corresponding Authors: Kunyue Leng (lengky@nwu.edu.cn), Lirong Zheng (zhenglr@ihep.ac.cn), Yunteng Qu (yuntengqu@nwu.edu.cn)

Abstract

Electrocatalytic acetylene semi-hydrogenation to ethylene powered by renewable electricity represents a sustainable pathway, but the inadequate current density and single-pass yield greatly impedes the production efficiency and industrial application. Herein, we develop a F-modified Cu catalyst that shows an industrial partial current density up to 0.76 A cm^{-2} with an ethylene Faradic efficiency surpass 90%, and the maximum single-pass yield reaches a notable 78.5%. Furthermore, the Cu-F showcase the capability to directly convert acetylene into polymer-grade ethylene in a tandem flow cell, almost no acetylene residual in the production. Combined characterizations and calculations reveal that the $Cu^{\delta+}$ (near fluorine) enhances the water dissociation, and the generated active hydrogen are immediately transferred to Cu^{0} (away from fluorine) and react with the locally adsorbed acetylene. Therefore, the hydrogen evolution reaction is surpassed and the overall acetylene semi-hydrogenation performance is boosted. Our findings provide new opportunity towards rational design of catalysts for large-scale electrosynthesis of ethylene and other important industrial raw.

Introduction

Ethylene (C_2H_4), as a primary building block for polyethylene, meets a vast annual consumption [1]. At present, industrial-scale production of C_2H_4 is still dominated by the petroleum cracking, which needs consume the finite petroleum reserves accompanying with high energy consumption [2-3]. Recently, coal-derived acetylene followed by thermal semihydrogenation (SAE) is recognized as a promising route to C_2H_4 production [4-6]. However, the SAE process suffers from excess hydrogen consumption, high reaction temperature, and pressure [7-9]. Furthermore, an additional acetylene removal step may need to satisfy the stern requirement of acetylene content in polymer-grade ethylene (not exceeding 5 ppm). Electrocatalytic SAE (ESAE) powered by renewable electricity provides a sustainable alternative route to directly transform acetylene to polymer-grade ethylene [10-13]. Moreover, ESAE process adopts water (H_2O) as the hydrogen source, avoiding the consumption of H_2. Nevertheless, the severe hydrogen evolution reaction (HER) at industrial-level current density greatly restricts the Faraday efficiency (FE) and the one-path yield of C_2H_4. In this case, the large recycle ratio is required to completely convert C_2H_2 to C_2H_4, thus greatly increase the production cost and compress the profit margin of ESAE. Actually, a fundamental demand in becoming ESAE profitable is a 85% or more FE of C_2H_4 at a current density of 0.2 A cm^{-2} or more [14]. Therefore, the rational design and fabrication of catalysts that can suppress HER and efficiently produce ethylene at industrial-level current densities is urgently desired.

The research on ESAE can be traced back to the 1970s [15], which was limited by poor solubility of acetylene and insufficiently effective catalysts. Very Recently, Cu-based catalysts have been demonstrated to be prospective candidates for realizing the selective electrocatalytic semihydrogenation of acetylene [16-18]. Moreover, the issue of solubility has been addressed by utilizing gas diffusion layer (GDL) electrodes, which can improve mass transfer by creating a gas-liquid-solid interface [19-21]. However, the competing HER still greatly reduce the FE of C_2H_4 once the current density exceed 0.1 A cm^{-2}. In this regard, nanoscale copper catalyst (5 nm) with unsaturated Cu sites were developed and performed strong suppressive HER (<4%) during ESAE at industrial-level current density (0.2-0.5 A cm^{-2}) [22]. Despite significant progress has been achieved, the precise control of the size and crystal structure of nanoscale Cu catalysts may increase potential materials cost during industrial

application of ESAE. Inspired by catalyst design for CO_2 electroreduction reaction, modulating the local electronic structure of copper by non-metal modifying can efficiently boost reaction kinetics [23-25]. Furthermore, it has been demonstrated the introduction of non-metal, such as fluorine, boron, into Cu achieved robust suppressive HER performance at an industrial-level current density (surpass 1 A cm^{-2}) [26-29]. Therefore, reasonably constructing non-metal modifying Cu catalysts onto a GDL coated carbon paper electrode are supposed to realize the industrial application of ESAE but remains challenges.

Herein, we develop halogen-doped Cu catalysts through an in-situ electrical reduction method for achieving efficient ESAE process. Detailed physical characterizations of the catalysts reveal that halogen atoms are adsorbed onto the Cu (111) plane through halogen-Cu bonding. Among these catalysts, the F-doped catalyst (Cu-F) demonstrate superior performance in ESAE when working in the flow cell. The current density reaches a remarkable 1 A cm^{-2} at -1.5 V (vs. RHE), and the FE of ethylene surpass 90% at a broad potential range from -0.5 to -1.3 V (vs. RHE). Notably, Cu-F showcase the capability to directly convert acetylene (70 mol% in Ar) into polymer-grade ethylene in a tandem flow cell device. The experimental verification combined with the DFT calculations reveals the boosting of water dissociation on the Cu sites near the F atom, resulting the generation of active hydrogen, which are transferred to the Cu far from F and react with the adsorbed acetylene. Thus, the HER is suppressed and the overall ESAE is promoted over Cu-F.

Results

Preparation and characterization of Cu-F catalyst

In this study, the electrocatalyst is synthesized by in-situ electrical reduction using halogen-containing copper as precursor (Figure 1a). Typically, the preparation of the Cu-F involves treating $Cu(NO_3)_2$ and NH_4HF_2 in DMF via a solvent-thermal process, resulting in a green powdery precursor of Cu(OH)F (Figure S1-S3). Then the Cu(OH)F is coated onto a GDL and reduced at a potential of -1.6 V (vs. Ag/AgCl). The resultant Cu-F catalysts are separated from the GDL for further characterization. SEM and TEM images of Cu-F reveal the aggregation of irregular nanoparticles with a size ranging from 45-90 nm, which exhibit distinct crystalline characteristics (Figure 1b and Figure S4). The EDS element mapping confirm the uniform distribution of F on the Cu particles (Figure 1c), with the F content of 15.6 atomic% (Table S1).

Aberration-corrected HAADF-STEM is used to identify the surface structure of Cu-F. Figure 1d clearly illustrates the presence of Cu atomic alloy in Cu-F, with a lattice spacing measured at 0.208 nm corresponding to the Cu (111) plane. This observation was further confirmed by characteristic diffraction peaks of metallic Cu in Figure 1e. Moreover, no obvious lattice distortion caused by heteroatomic insertion is observed in HAADF-STEM image, combined with the F 1*s* XPS spectra (Figure S5), indicating the adsorption of F onto the surface crystalline Cu.

The linear sweep voltammetry (LSV) curve of Cu(OH)F reduction shows a peak at -0.35 V vs. RHE (Figure S6), indicating the occurrence of the electroreduction on Cu^{2+} during the Cu-F generation. The Cu 2*p* XPS spectra (Figure S7) further confirm that Cu-F exhibits a binding energy for Cu $2p_{3/2}$ at 932.7 eV, slightly higher than that reported 932.4 eV for Cu^0 [30]. Additionally, the Cu LMM spectra (Figure S8) indicate the coexistence of Cu^0 and $Cu^{\&+}$ in the Cu-F catalyst. X-ray absorption spectroscopy (XAS) was used to further investigate the oxidation state and coordination of Cu in Cu-F. The XANES spectra at the Cu K-edge indicate that the oxidation state of Cu in Cu-F is between 0 and +1 (Figure 1f). The linear simulation of edge energy and oxidation state provides insight into the average oxidation state of Cu in Cu-F, which was approximately +0.2 (Figure S9). This slight positive oxidation state could be attributed to the presence of $Cu^{\&+}$ induced by the interaction of Cu and F. The combination of Cu and F is further explored by Cu K-edge FT EXAFS in Figure 1g, which showed a dominant peak at ~2.19 Å corresponding to the Cu-Cu coordination. Additionally, a peak at ~1.56 Å is observed over Cu-F, situates between the Cu-O coordination in CuO and the Cu-F coordination in CuF_2. This observation in agreement with the wavelet-transform images (Figure 1h-j and Figure S10), indicating the partial coordination of Cu with F in the Cu-F catalyst. Furthermore, the pure crystalline Cu (Cu NP) and Cl, Br, I doped Cu catalysts (Cu-Cl, Cu-Br and Cu-I) are also prepared and investigated in this work (Figure 1e and Figure S11-14).

Electrocatalytic acetylene semi-hydrogenation

The ESAE evaluation is conducted by a flow cell device with an electrode area of $1cm^{-2}$ (Figure S15). Subsequently, 1 M KOH and C_2H_2/Ar gas (70 mol%) are pumped into the flow cell respectively at the flow rate of 1 and 30 ml min^{-1}. (The addition of argon to the C_2H_2 gas was intended to protect the chromatographic system.). To ensure consistency, all potentials used in the experiment were converted to the RHE

reference without solution resistance compensation, except the long-term stability test of Cu-F.

As disclosed by the LSV curves (Figure 2a), Cu-based catalysts show obviously higher current density when exposed to C_2H_2 than to Ar, confirming their intrinsic activity for ESAE. Additionally, the halogen doping noticeably enhances the ESAE performance of Cu, with the current density increasing along the electronegativity. As result, the Cu-F shows the best ESAE performance with the current density surpasses 1 A cm^{-2} at -1.5 V (vs. RHE). The ECSA-normalized current densities follow the same trend with the apparent ESAE performance (Figure S16-17, Table S2), ruling out the effect of the morphology, and demonstrating the superior intrinsic activity of Cu-F. The single-pass C_2H_2 conversion over Cu-F reaches 30.3 %, which increases to 78.5% when reducing the flow rate to 6 ml min^{-1}, and the LSV curves show no obvious change with the flow rate (Figure S18). Ethylene (C_2H_4) is identified as the main production, accompanied by few H_2 and C_4, no liquid production is detected (Figure S19-20). The partial current density for C_2H_4 is indicated up to 794.8 mA cm^{-2} at the potential over -1.5 V (vs. RHE, Figure 2b). Moreover, the Cu-F shows a remarkable onset potential of -0.121 V (at 0.1 mA cm^{-2}) for C_2H_4 (Figure S21), -0.607 V greater than that for the competing HER, demonstrating no external H_2 is required for producing C_2H_4. The notable C_2H_4 selectivity of Cu-F in alkaline medium is revealed by the high Faraday efficiency (FE), which surpass 90% at a wide potential range from -0.5 to -1.3 V (vs. RHE, Figure 2c, Figure S22), better than the Cu NP (~80%) and other halogen dopped Cu (Figure S23-26). In the same potential range, the highest H_2 FE over Cu-F is just 4.1% (-1.3 V), but for Cu NP it reaches 28.9% (-1.0 V). The superior current density and C_2H_4 selectivity led to a high C_2H_4 formation rate of 1 mol h^{-1} cm^{-2} at -1.0 V (vs. RHE, Figure 2d), making it as one of the best catalysts for ESAE (Table S3). It is worth noting that ESAE performance of Cu-F negligible decay in 43 h at a current density of 200 mA cm^{-2} (Figure 2e and Figure S27), and the used Cu-F maintain the original structure (Figure S28), demonstrating its robust long-term stability. It is inevitable that part of F will leach into the electrolyte during the in-situ electrical generation of Cu-F from Cu(OH)F. Figure S29 shows the ESAE performance of Cu-F in a fresh electrolyte (F-free), the negligible changes on the activity exclude the effect of the solvated fluoride on the ESAE process.

Mechanistic insight

The nature of the active sites in Cu-F during the ESAE process is investigated by in-situ XAFS (Figure S30). The freshly generated Cu-F (5 min in Ar) shows an average oxidation state of Cu between 0 to +1 with Cu-Cu and F-Cu coordination, confirming the innate Cu^{+} sites accompany Cu^{0} sites. Moreover, after triggering the ESAE by switch the gas flow to C_2H_2 for 120 min, the average oxidation state and coordination environment of Cu show slight changes, suggesting the maintaining of the F-Cu interaction. Considering the much more positive onset potential of ESAE (-0.12 V, Figure S21) than the reduction potential of $Cu^{\&+}$ (-0.23 V, Figure S6), C_2H_2 is much easier to be reduced than $Cu^{\&+}$. Therefore, the F-Cu coordination is protected from being deeply reduced, which contributes to the superior ESAE performance of Cu-F.

To elucidate the mechanism underlying the superior performance of Cu-F, ESAE pathway is firstly studied using potential-dependent operando Raman spectra (Figure S31). As shown in Figure 3a, the two peaks at 1127 and 1513 cm^{-1} can be assigned to the C-C and C≡C vibrations of polyacetylene [22]. The signal belonging to the C≡C vibration is detected at ~1700 cm^{-1} at an open circuit potential (OCP), indicating the adsorption of acetylene on Cu-F[18]. This signal disappears when the potential increase to -0.4 V (vs. RHE), and new signals belonging to bonded ethylene emerge at ~1343 and ~1554 cm^{-1} [14, 18], which confirm the occurrence of ESAE process on Cu-F. Furthermore, the signals of ethylene on Cu-F can be observed at wide potential range from -0.4 to -1.0 V (vs. RHE). In contrast, the Raman signal for ethylene over Cu NP becomes indistinguishable at a potential larger than -0.8 V (vs. RHE, Figure 3b), which should be attributed to the intense hydrogen generation at high potential. Interestingly, the LSV curves in pure Ar show that Cu-F exhibits better HER activity compared to Cu NP (Figure 2a). However, the FE of H_2 over Cu-F is much lower than that over Cu NP, suggesting the suppression of HER over Cu-F in ESAE process due to rapid $^{*}H$ consumption.

The pH of the electrolyte is investigated to reveal the hydrogen source in the ESAE. As reported by Deng et al., a typical electron-coupled proton transfer process ($^{*}C_xH_y + H_2O + e^{-} \rightarrow {}^{*}C_xH_{y+1} + OH^{-}$) is more favorable under relative low pH [20]. However, the pH shows insignificant effect on the overall FE of Cu-F (Figure S32-34), which excludes the electron-coupled proton transfer process. The hydrogenation of C_2H_2 is preferentially facilitated by the surface absorbed $^{*}H$, which stem from the water

dissociation. The surface $^{*}H$ is further judged by adding of *tert*-Butanol (*t*-BuOH) into the electrolyte. The *t*-BuOH can capture $^{*}H$ to form inert 2-methyl-2-propanol radicals, leading to a suppressed hydrogenation activity [31-32]. As shown in Figure S35, the Cu-F displays inferior performance after adding *t*-BuOH, confirming the participation of surface $^{*}H$ in the hydrogenation of C_2H_2. To gain insights into the role of water dissociation in $^{*}H$ generation, the kinetic isotope effect (KIE) of H/D in studied during ESAE. The Cu NP shows a KIE of 2.01 (Figure 3c and Figure S36), which is characteristic of primary KIE, indicating the involvement of water dissociation in the rate-determining step (RDS) [29]. For Cu-F, the KIE decrease to 1.26, water dissociation is no longer involved in the RDS, demonstrating that Cu-F accelerates the hydrogen transfer process via promoting water dissociation [33].

The effect of hydrated cation $M^{+}(H_2O)_n$ (n represent the number of hydrations) in electrolyte is investigated to deeply insight the active sites for water dissociation. The hydrated cation would interact with the surface F in the Helmholtz layer, contributing to the dissociation of H_2O to form active hydrogen species, and this interaction is determined by the n and radius of the hydrated cation [34]. As shown in Figure 3d and Figure S37, when replacing 1 M KOH by 1 M tetramethylammonium hydroxide (TMAH) or NaOH, both the C_2H_2 conversion and HER over Cu-F exhibit significant decay, which due to the weaker interaction of F with TMAH and $Na^{+}(H_2O)_{13}$ than with $K^{+}(H_2O)_7$, caused by their larger radius and n [29, 34]. In contrast, no obvious change on C_2H_2 conversion and HER over Cu NP are observed, although cations with different nature (such as different diffusion coefficient) are used (Figure S38). The investigation of hydrated cation reveals the key role of F doping for regulating water dissociation.

The DFT calculation is employed to further understand the ESAE process on Cu-F. In order to clarify the role of F atom, three different active sites are simulated, $Cu^{\delta+}$ site near the F atom in Cu-F (Cu(111)-F-*near*), Cu^0 site far from the F atom in Cu-F (Cu(111)-F-*far*) and Cu^0 sites in pure crystalline copper (Cu (111)) (Figure S39-40). The adsorption energy (E_{ad}) of C_2H_2 and H_2O are firstly studied. As shown in Figure 3e, the E_{ad} of C_2H_2 on Cu (111)-F-near is much higher than that on Cu (111)-F-*far*, indicating the C_2H_2 is more favorable to be adsorbed on the Cu sties far form F atom than the Cu nearby. On the other hand, Cu (111)-F-*near* shows priority adsorption of H_2O versus C_2H_2 confirmed by its lower E_{ad} for H_2O than C_2H_2. As results, the strong interaction between $^{*}H_2O$ and Cu (111)-F-*near* significantly promote the water

dissociation (Figure 3f), and boost the generation of active H species. Furthermore, the unfavorable $^{*}H$ adsorption on Cu (111)-F-*near* may enable the H transferring to Cu (111)-F-*far* (Figure 3g), the low H transfer energy barrier of 0.105 eV further confirms the ease of transferring (Figure S41). Accordingly, an ESAE process includes hydrogen-localization transfer can be illustrated in Figure 3h. Namely, H_2O firstly absorb and dissociate on the Cu (111)-F-*near*, then the generated active H species are transferred to the Cu sites far from the F atom and react with the adsorbed C_2H_2, ultimately generate the C_2H_4 production. As shown in Figure 3i, the rate determining step for the as illustrated C_2H_2 hydrogenation process on Cu sites is identified as the hydronation of $^{*}C_2H_2$ to $^{*}C_2H_3$. The Cu (111)-F-*far* shows a reaction barrier of 0.12 eV at 0 V vs. RHE, which is reduced to 0.09 eV at -1.0 V vs. RHE (Figure S42), demonstrating the promotion of electrochemical steps by adjusting the applied potential. Moreover, the C_2H_2 semi-hydronation barrier of Cu Cu (111)-F-*far* is lower than both the C_2H_2 semi-hydronation barrier of Cu (111) (0.21 eV), and the H_2 generation barrier of itself (0.29 eV, Figure S43). Thus, the HER process is suppressed, and the overall ESAE process is promoted over Cu-F.

Direct electroreduction of acetylene to polymer-grade ethylene

Motivated by the impressive FE for C_2H_4 and high current density exhibited by Cu-F, this study explores the direct conversion of C_2H_2 (70 mol% in Ar) to polymer-grade C_2H_4 using Cu-F. It is essential to consider the effect of low C_2H_2 partial pressure and the C_2H_4-rich environment on the ESAE process, as the C_2H_2 impurities in polymer-grade C_2H_4 must be below 5 ppm [35]. Figure S44 demonstrates that the current density and FE for C_2H_4 decrease with the reduction in the C_2H_2 concentration, particularly at a low concentration of 1 mol%. Despite this, when ESAE is performed using a 25 cm^2 flow cell (electrode area: 25 cm^2) with 1 mol% C_2H_2 in C_2H_4 (Figure S45), remarkable C_2H_2 conversion and C_2H_4 selectivity are still achieved (Figure 4a and Figure S46-47). Furthermore, the residual C_2H_2 in the outlet gas remains below 5 ppm for up to 13.5 hours at an applied cell voltage (E_{cell}) of -2.2 V (Figure 4b). This demonstrates the efficient ESAE capability of Cu-F, even in a C_2H_4-rich environment with a low C_2H_2 partial pressure.

The direct electroreduction of acetylene to polymer-grade ethylene is performed using a custom-made tandem device consisting of a 1 cm^2 flow cell and a 25 cm^2 flow cell (Figure S48). The designing is based on the capacity of the 1 cm^2 flow cell to deal

with high concentration C_2H_2 feed gas, and the ability of the 25 cm^2 flow cell for converting residual C_2H_2 at low concentration. Initially, C_2H_2 (70 mol% in Ar) is pumped into the 1 cm^2 flow cell, and the outlet gas is then immediately introduced into the 25 cm^2 flow cell without any purification (Figure 4c). The optimal flow rate is determined to be 6 ml min^{-1}, as it achieves a high single-pass C_2H_2 conversion of approximately 80% and C_2H_4 selectivity over 90% in the 1 cm^2 flow cell (Figure S18 and S49). As shown in Figure 4d, the current density over Cu-F reaches 500 mA cm^{-2} in the 1 cm^2 flow cell and 20 mA cm^{-2} in the 25 cm^2 flow cell, maintaining stability for up to 3 h without significant decay. Furthermore, minimal residual C_2H_2 is detected in the final C_2H_4 production, and the carbon loss in the tandem device is negligible (Figure 4c and Figure S50). The high current density, robust stability, and high C_2H_4 selectivity of Cu-F in the tandem device highlight its potential application for the direct generation of polymer-grade ethylene from acetylene on an industrial scale.

In summary, halogen-doped Cu catalysts have been prepared as efficient electrocatalysts for the semi-hydrogenation of acetylene to ethylene. The optimized Cu-F catalyst, featuring F atoms adsorbed on the Cu (111) plane, exhibits outstanding performance in acetylene electroreduction. It achieves a current density of 1 A cm^{-2} at a potential of -1.5 V (vs. RHE), and the Faraday efficiency for ethylene exceeds 90% over a wide potential range from -0.5 to -1.3 V (vs. RHE). Additionally, the single-pass acetylene conversion varies between 30% and 80% depending on the flow rate. In-situ spectroscopy, in combination with DFT calculations, reveals that the presence of F atoms enhances the water dissociation ability of adjacent Cu sites. This promotes the generation of active hydrogen species that are subsequently transferred to the adsorbed acetylene, thereby boosting the ESAE pathway. Furthermore, the Cu-F catalyst demonstrates almost complete conversion of acetylene (70 mol% in Ar) to ethylene in a tandem flow cell device, highlighting its significant potential for direct electroreduction of acetylene into polymer-grade ethylene. This study opens new opportunities for the rational design of catalysts for large-scale electrosynthesis of ethylene and other essential industrial raw materials.

Methods

Preparation of Cu(OH)F. Cu(OH)F was prepared according to previously report [29]. Typically, 114.1 mg (2 mmol) NH_4HF_2 was dispersed in 50 mL DMF with vigorous stirring at room temperature for at least 40 min, then the solution

correspondingly changed to blue after 483.2 mg (2.0 mmol) $Cu(NO_3)_2 \cdot 3H_2O$ was introduced and stir for 30 min. The homogeneous liquid was poured into 100 ml hydrothermal reactor and sealed, then heated at 160 °C for 4 h. The green powder was collected by employing centrifuge process with ethanol and water washing in turn three times after it cooled down. After dried at 60 °C in vacuum, Cu(OH)F is obtained.

Preparation of Cu-F gas diffusion electrode. The working electrode was prepared through in-situ electro-derivation of the relevant precursor on GDL surrounding 1 M KOH. Here, take the process of fabricating Cu-F GDE as an example. 5 mg Cu(OH)F precursor was dispersed in 0.75 ml C_2H_5OH/H_2O (v/v, 1:1) with 25 μl nifion binder, then uniform suspension ink was formed by ultrasonic dispersion method within 1 h. Afterward, all ink spray onto 0.5x2.0 cm GDL on the top of a heating plat at 65 ^oC to evaporate solvent with mas loading controlled at 1.0-1.2 mg. For 5x5 cm GDE, Cu(OH)F mass loading was about 25.0-30.1 mg. GDL with loading Cu(OH)F precursor as working electrode was in-situ reduced in a flow-cell and was immersed in Ar (30 ml min^{-1}) and 1M KOH at 1.6 V (vs. Ag/AgCl) for 300 s. The obtained catalyst was labeled as Cu-F.

More details are shown in the supporting information file.

Data availability

The data that support the findings of this study are available within the article and its Supplementary Information files. All other relevant data supporting the findings of this study are available from the corresponding authors upon reasonable request. Source Data are provided with this paper.

References

1. Guo, W. et al. Visualization of on-surface ethylene polymerization through ethylene insertion. *Science* **375**, 1188-1191 (2022).
2. Bodke, A. S., Olschki, D. A., Schmidt, L. D., & Ranzi, E. High selectivities to ethylene by partial oxidation of ethane. *Science* **285**, 712-715 (1999).
3. Gao, Y. et al. Recent advances in intensified ethylene production-a review. *ACS Catal.* **9**, 8592-8621 (2019).
4. Schobert, H. Production of acetylene and acetylene-based chemicals from coal. *Chem. Rev.* **114**, 1743-1760 (2014).
5. Liu, Y. et al. Polyoxometalate-based metal-organic framework as molecular

sieve for highly selective semi-hydrogenation of acetylene on isolated single Pd atom sites. *Angew. Chem. Int. Edit.* **60**, 22522-22528 (2021).

6. Studt, F. et al. Identification of non-precious metal alloy catalysts for selective hydrogenation of acetylene. *Science* **320**, 1320-1322 (2008).
7. Jiao, X. et al. Conversion of waste plastics into value-added carbonaceous fuels under mild conditions. *Adv. Mater.* **33**, 2005192 (2021).
8. Wang, K. et al. Highly selective catalytic oxi-upcycling of polyethylene to aliphatic dicarboxylic acid under a mild hydrogen-free process. *Angew. Chem. Int. Edit.* e202301340 (2023).
9. Abakumov, A. A. et al. Catalytic properties of reduced graphene oxide in acetylene hydrogenation. *Carbon* **157**, 277-285 (2020).
10. Otsuka, K. & Yagi, T. An electrochemical membrane reactor for selective hydrogenation of acetylene in abundant ethylene. *J. Catal.* **145**, 289-294 (1994).
11. Ma, W. et al. π-adsorption promoted electrocatalytic acetylene semihydrogenation on single-atom Ni dispersed n-doped carbon. *J. Mater. Chem. A* **10**, 6122-6128 (2022).
12. Ling, Y. et al. Selenium vacancy promotes transfer semihydrogenation of alkynes from water electrolysis. *ACS Catal.* **11**, 9471-9478 (2021).
13. Liu, Z. et al. Metal phthalocyanines as efficient electrocatalysts for acetylene semihydrogenation. *Chem. Eng. J.* **431**, 134129 (2022).
14. Zhao, B. H. et al. Economically viable electrocatalytic ethylene production with high yield and selectivity. *Nat. Sustain.* DOI: 10.1038/s41893-023-01084-x (2023) (2023).
15. Davitt, H. J. & Albright, L. F. Electrochemical hydrogenation of ethylene, acetylene, and ethylene-acetylene mixtures. *J. Electrochem. Soc.* **118**, 236 (1971).
16. Zhang, L. et al. Efficient electrocatalytic acetylene semihydrogenation by electron-rich metal sites in n-heterocyclic carbene metal complexes. *Nat. Commun.* **12**, 6574 (2021).
17. Huang, B., Durante, C., Isse, A. A. & Gennaro, A. Highly selective electrochemical hydrogenation of acetylene to ethylene at Ag and Cu cathodes. *Electrochem. Commun.* **34**, 90-93 (2013).
18. Bu, J. et al. Selective electrocatalytic semihydrogenation of acetylene

impurities for the production of polymer-grade ethylene. *Nat. Catal.* **4**, 557-564 (2021).

19. Shi, R. et al. Room-temperature electrochemical acetylene reduction to ethylene with high conversion and selectivity. *Nat. Catal.* **4**, 565-574 (2021).
20. Wang, S. et al. Highly efficient ethylene production via electrocatalytic hydrogenation of acetylene under mild conditions. *Nat. Commun.* **12**, 7072 (2021).
21. Zhu, K. et al. Unraveling the role of interfacial water structure in electrochemical semihydrogenation of alkynes. *ACS Catal.* **12**, 4840-4847 (2022).
22. Xue, W. et al. Electrosynthesis of polymer-grade ethylene via acetylene semihydrogenation over undercoordinated cu nanodots. *Nat. Commun.* **14**, 2137 (2023).
23. Nitopi, S. et al. Progress and perspectives of electrochemical CO_2 reduction on copper in aqueous electrolyte. *Chem. Rev.* **119**, 7610-7672 (2019).
24. Wang, X. et al. Gold-in-copper at low $^{*}CO$ coverage enables efficient electromethanation of CO_2. *Nat. Commun.* **12**, 3387 (2021).
25. Xu, Y. et al. Low coordination number copper catalysts for electrochemical CO_2 methanation in a membrane electrode assembly. *Nat. Commun.* **12**, 2932 (2021).
26. Fang, M. et al. Hydrophobic, ultrastable $Cu^{\delta+}$ for robust CO_2 electroreduction to C_2 products at ampere-current levels. *J. Am. Chem. Soc.* **145**, 11323-11332 (2023).
27. Barhacs, B., Janssens, E. & Hoeltzl, T. C_2 product formation in the CO_2 electroreduction on boron-doped graphene anchored copper clusters. *Phys. Chem. Chem. Phys.* **24**, 21417-21426 (2022).
28. Zhou, Y. et al. Dopant-induced electron localization drives CO_2 reduction to C_2 hydrocarbons. *Nat. Chem.* **11**, 1167-1167 (2019).
29. Ma, W. et al. Electrocatalytic reduction of CO_2 to ethylene and ethanol through hydrogen-assisted C-C coupling over fluorine-modified copper. *Nat. Catal.* **3**, 478-487 (2020).
30. Ma, S. et al. Ionic exchange of metal-organic frameworks for constructing unsaturated copper single-atom catalysts for boosting oxygen reduction reaction. *Small* **16**, 2001384 (2020).

31. Liu, H. et al. Deep dehalogenation of florfenicol using crystalline CoP nanosheet arrays on a Ti plate via direct cathodic reduction and atomic H. *Environ. Sci. Technol.* **53,** 11932-11940 (2019).
32. Wu, Y., Liu, C., Wang, C., Lu, S. & Zhang, B. Selective transfer semihydrogenation of alkynes with H_2O (D_2O) as the H (D) source over a Pd-P cathode. *Angew. Chem. Int. Edit.* **59**, 21170-21175 (2020).
33. Chen, S. et al. Unveiling the proton-feeding effect in sulfur-doped Fe-N-C single-atom catalyst for enhanced CO_2 electroreduction. *Angew. Chem. Int. Edit.* **61**, e202206233 (2022).
34. Guo, S. et al. Electrocatalytic hydrogenation of quinolines with water over a fluorine-modified cobalt catalyst. *Nat. Commun.* **13**, 5297 (2022).
35. Jiang, X. et al. Cu single-atom catalysts for high-selectivity electrocatalytic acetylene semihydrogenation. *Angew. Chem. Int. Edit.* e202307848 (2023).

Acknowledgements

The authors thank the photoemission endstation beamline 1W1B station in the Beijing Synchrotron Radiation Facility (BSRF) for help with the characterizations. This work is financially supported by the National Natural Science Foundation of China (22275147 to Y. Q., 52301289 to K. L., and 21902150 to Y. Q.), Natural Science Basic Research Program of Shaanxi (2022JQ-082 to K. L. and 2022JM-018 to Y. W.).

Author Contributions

Y. Qu and K. Leng designed the experiments and performed DFT calculation. L. Bai, Y. Wang and Z. Han conducted the experiments and performed the catalysts. L. Zheng performed X-ray absorption fine structure spectra measurements. All author contributed to the scientific interpretation and we sincerely thank J. Bai and Y. Wu for profound suggestions and insightful guidance.

Competing interests

The authors declare no competing interests.

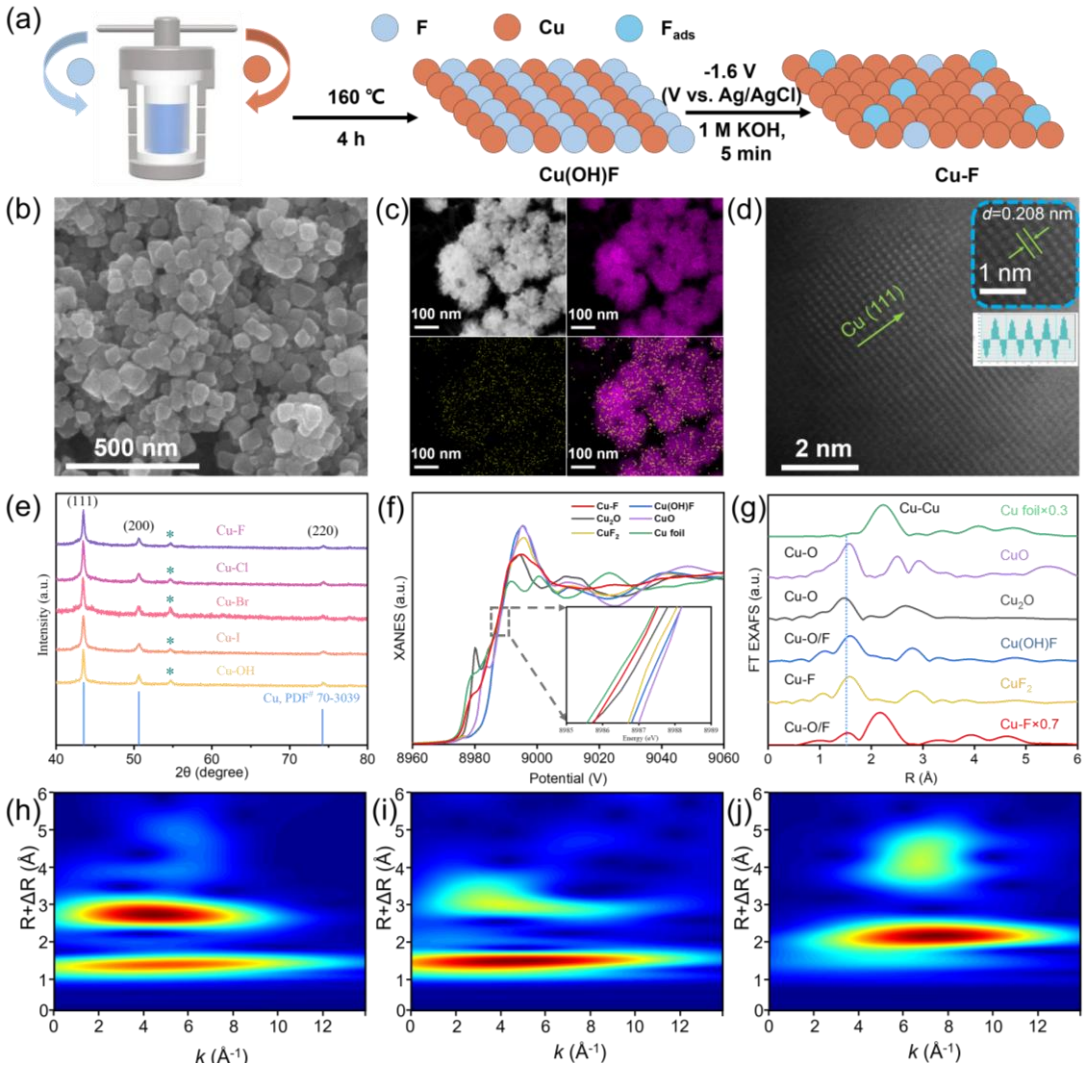

Figure 1. Structure identification of Cu-F. (a) Illustrated synthesis process. (b) SEM image. (c) EDS element mapping. (d) Aberration-corrected HAADF-STEM image. (e) XRD patterns. (f) XANES spectra with reference samples. (g) FT EXAFS spectra with reference samples. (h-j) Wavelet transformations of Cu_2O, CuF_2 and Cu-F.

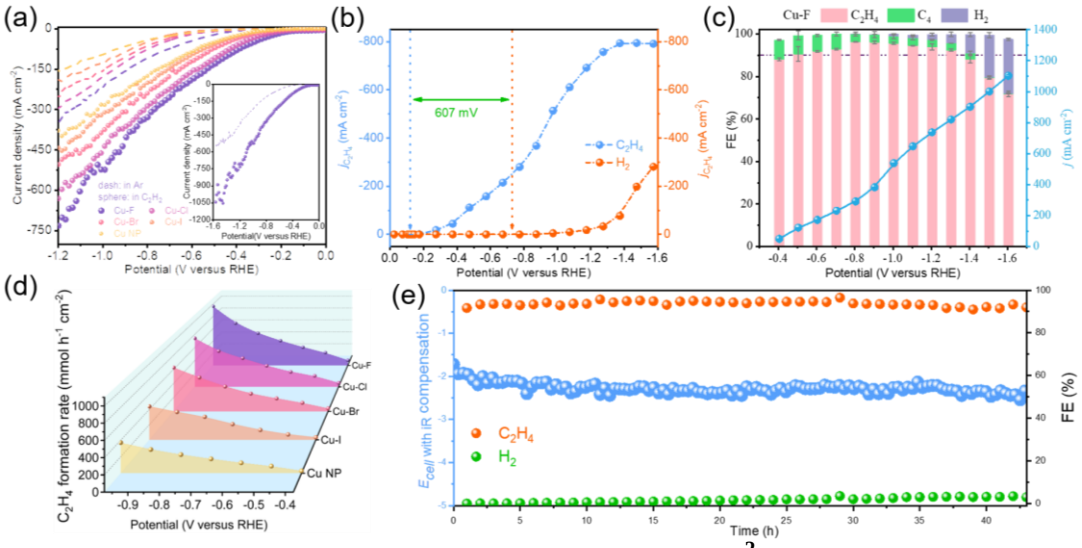

Figure 2. Electrocatalytic performance of Cu-F in 1 cm^2 flow cell. (a) LSV curves in Ar and 70% C_2H_2/Ar. (b) partial current density for C_2H_4 and H_2. (c) Faraday efficiency for C_2H_4 and H_2 at various potential and the corresponding current density, the maximum measurement error is ±5%. (d) C_2H_4 formation rate. (e) long-term stability at a constant current density of 200 mA cm^{-2}. All tests are measured using a three-electrode flow cell (1 cm^2) in 1 M KOH at room temperature under 70 mol% C_2H_2/Ar flow (30 ml min^{-1}). The results are presented without iR compensation except e. For e the R=9.4 Ω.

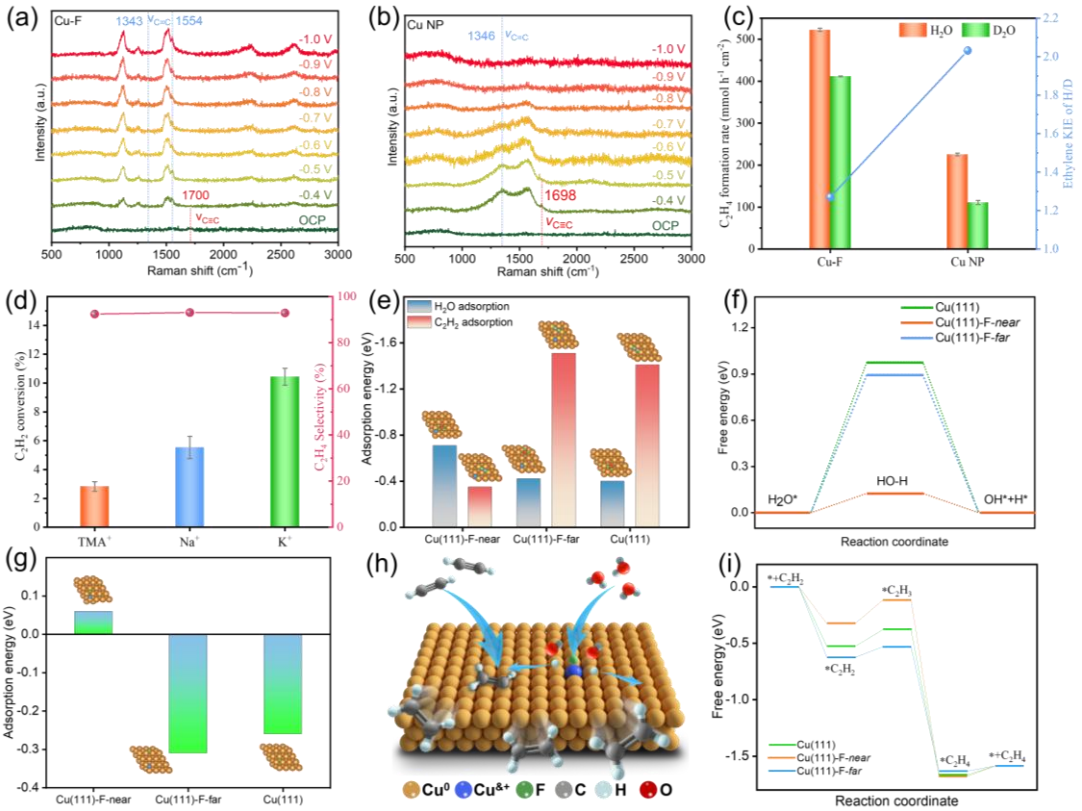

Figure 3. Mechanistic insight. (a, b) Potential-dependent operando Raman spectra, measured using a three-electrode observable cell in 1 M KOH at room temperature under 70 mol% C_2H_2/Ar flow (30 ml min^{-1}). (c) Kinetic isotope effect, KIE, the maximum measurement error is ±4.8%. (d) C_2H_2 conversion under 70 mol% C_2H_2/Ar flow (30 ml min^{-1}) in 1 M KOH, NaOH and TMAH electrolyte. (e) Adsorption energy for C_2H_2 and H_2O, (f) free energy diagram for water dissociation and (g) adsorption energy for hydrogen, at 0 V vs. RHE. (h) Schematic illustration of the ESAE pathway over Cu-F. (i) Free energy diagram for the hydrogenation of C_2H_2 at 0 V vs. RHE.

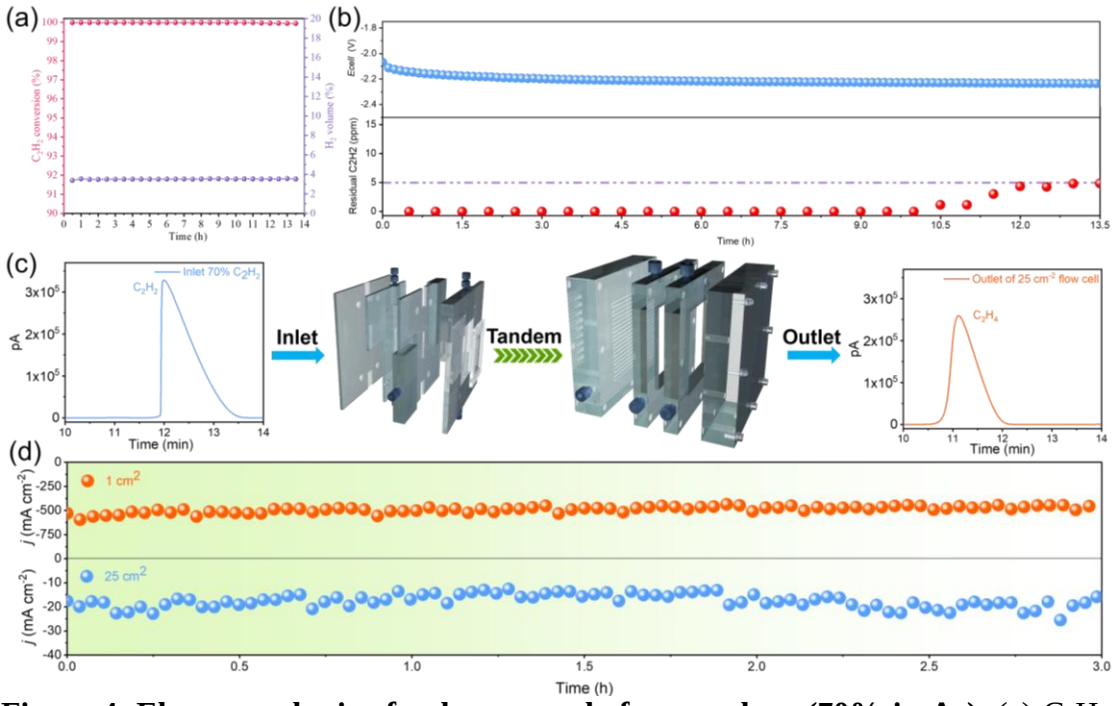

Figure 4. Electrosynthesis of polymer-grade for acetylene (70% in Ar). (a) C_2H_2 conversion and (b) long-term operation of ESAE over Cu-F under ethylene-rich environment, measured using a three-electrode flow cell (25 cm^2) in 1 M KOH at room temperature under 1 mol% C_2H_2/C_2H_4 flow (20 ml min^{-1}), constant current density set as 40 mA cm^{-2}. (c) Schematic of the tandem flow cells and the chromatograms at different locations of the gas line. (d) Long-term operation of ESAE in the tandem flow cells, 70 mol% C_2H_2 in Ar, flow rate 6 ml min^{-1}, constant potentials set as -1.1 and -0.6 V (vs. RHE) for 1 cm^2 and a 25 cm^2 flow cells, respectively.